Article

Ultra–Short-Term Reproducibility of Speckle-Noise Freed Fluid and Tissue Compartmentalization of the Choroid Analyzed by Standard OCT

Peter Maloca[1], Cyrill Gyger[1], Andreas Schoetzau[2], and Pascal W. Hasler[1]

[1] Department of Ophthalmology, University of Basel, Basel, Switzerland
[2] Department of Biomedical Statistics, University of Basel, Basel, Switzerland

Correspondence: Peter Maloca, OCT research laboratory OCTlab, Department of Ophthalmology, University of Basel, Mittlere Strasse 91, CH-4056 Basel, Switzerland. e-mail: info@dr-maloca.ch

Purpose: We measured reproducibility of speckle-noise freed fluid and tissue compartmentalization of the choroid (choroidal angiography and tissue characterization).

Methods: This study included 26 eyes of 13 healthy females: 13 were used for repeated measurements and 13 were used for side comparison. A semiautomated algorithm removed speckle-noise with structure preservation.

Results: Intraclass correlation (ICC), with respect to reproducibility of the method, showed an ICC for choroidal fluid inner space analysis (FISA) of 95.15% (90.01–98.24). The ICC of tissue inner space analysis (TISA) was 99.75% (99.47–99.91). The total choroid ratio (TCR), calculated from volumes of tissue to vessels, showed an ICC of 88.84% (78.28–95.82). Comparison of eyes (left to right) showed a difference for FISA of 0.033 (95% confidence interval [CI] −0.0018–0.0680, $P = 0.063$), TISA −0.118 (CI −0.2373–0.0023, $P = 0.055$), and TCR −0.590 (CI −0.9047 to −0.2754, $P = 0.004$). The ICC for FISA and TISA showed a trend in the difference comparing left and right eyes; however, TCR showed a significant difference between the eyes in the measured area ($P < 0.001$). Mean overall FISA was 0.58 mm^3 (range, 0.25–0.98 mm^3, SD = 0.14). Mean TISA was 3.45 mm^3 (range, 2.38–5.0 mm^3, SD 0.072). Mean TCR was 6.13 (overall range, 3.93–10.2, SD = 1.34).

Conclusions: Differences in choroidal layers between subjects were found mainly due to alterations in choroidal tissue. Reproducibility of speckle-noise freed choroidal angiography appeared excellent.

Translational Relevance: Speckle noise is a granular "noise" that appears in a wide range of medical imaging methods as ultrasonography, magnetic resonance, computer tomography, or optical coherence tomography (OCT). Findings from basic science about speckle noise were translated into a novel, medical image postprocessing application that can separate signal from speckle noise with structure preservation with high reproducibility and enhance medical imaging.

Introduction

The human choroid is a very dense network of vascular loops. Approximately 95% of the blood flow to the eye is directed to the uveal system, of which approximately 70% is diverted into the choroidal channels.[1,2] The extremely important role of the choroid appears to be linked to the avascular fovea because the place of the sharpest vision is 100% dependent on a healthy choroidal circulation. There-fore, the choroid can be considered as a central switchboard to supply essential metabolites and oxygen to the outer retinal zones and retinal pigment epithelium.

The introduction of optical coherence tomography (OCT) into ophthalmology has brought many new insights in diagnosis, monitoring, and therapeutic interventions to many retinal diseases. With the development of enhanced depth imaging (EDI), the sensitivity of OCT has been increased, and tissue penetration has been improved. Using the EDI mode,

it has not only been possible to image the vitreous and retina but to obtain high-resolution images from the choroid and lamina cribrosa.[3–7]

Many diseases, such as polypoidal choroidal vasculopathy, central serous retinopathy, (CSR), and age-related macular degeneration (AMD), seem to have their origin in the choroid or appear to be directly in touch with it. Recent studies using spectral domain optical coherence tomography (SDOCT) over a 6-month time period to visualize the choroid have shown a significant thinning of the subfoveal choroidal thickness in patients with treated neovascular AMD in contrast to eyes with dry AMD.[8] In chronic CSR, mean subfoveal thickness was found to be significantly enlarged by 505 μm, and even asymptomatic eyes were affected.[9] The benefit of photodynamic therapy (PDT) in CSR was monitored using OCT in several studies. It was possible to document a reduction of central and perifoveal choroidal thickness after PDT.[10]

In pediatric subjects, the macular choroidal thickness (260.4 μm) and volume (0.205 mm^3) were significantly higher than those values in adults (206.1 μm, 0.160 mm^3, respectively).[11] In children, myopic eyes demonstrated a significant average thinning of approximately 50 μm of the choroid compared to nonmyopic eyes.[12] A thinner choroid also was reported in myopic adults, suggesting a correlation between choroidal thinning and marked axial elongation with age.[13] Beside these long-term changes of central or total choroidal thickness, it was discovered that the choroid shows dynamic diurnal changes in primates and humans.[14–19] A typical diurnal thickness pattern of the choroid was found with a highest mean choroidal thickness of 372.2 μm at 9:00 AM that progressively decreased to 340.6 μm at 5.00 PM. The mean diurnal difference was 33.7 μm (±21.5 μm) with a range of 3 to 67 μm.[20]

In addition, in the water drinking test of 1000 mL water, the choroidal volume was increased by 6.4%.[21] These fluctuations of the choroid are of great importance as the diurnal or iatrogen-induced variation or changes with age must always be considered in the evaluation and assessment of physiological or pathological situations. Several techniques to improve the visualization of the choroid have been used as image averaging, EDI OCT, or the application of a longer wavelength (swept source OCT [SSOCT]).[22–26]

Segmentation of the choroid in unilateral intermediate AMD has shown significant submacular thinning of the Sattler's and Haller's layer.[27] Choroidal segmentation maps in patients with reticular pseudo-drusen demonstrated significant thinning of the choroidal thickness.[28,29]

In summary, OCT has demonstrated enhanced penetration into the choroid and better visualization of choroidal vessels. Numerous choroidal studies have been performed either on research devices or using advanced swept source technology, and have studied the total choroidal thickness or single-center thickness. Therefore, in our study we aimed to evaluate a novel, three-dimensional, post-processing algorithm to free OCT images from speckle noise with structural preservation that can be used in all standard commercially available OCT systems, and to define the ultra–short-term reproducibility of speckle-noise freed choroidal angiography and a choroid tissue–vessel ratio for the first time.

Methods

Subjects and Measurements

In this study, we prospectively recruited 13 healthy females for repeated OCT raster scanning on a commercially available, standard, SDOCT system. Exclusion criteria were any ocular pathology, including history of ocular trauma, intra- or extraocular surgery, familial eye diseases, or elevated IOP; medical history of smoking; any ocular or systemic medication; or coexisting systemic diseases, such as diabetes mellitus, hypertension, or cardiovascular disease. Inclusion criteria were age >18 years, emmetropia or less than 4 diopters of myopia or hyperopia, adequate media clarity for fundus imaging, good central fixation, and good visual acuity. All subjects underwent a comprehensive ophthalmologic examination to exclude any existing retinal or choroidal pathology and had a best visual acuity of 20/20 or better in both eyes. Axial length was measured once before OCT using the Carl Zeiss IOL Master 500 (Carl Zeiss Meditec, Jena, Germany). Blood pressure and pulse were measured on the right arm of sitting subjects, using a fully automatic blood pressure device (Omron, M10-IT; OMRON Healthcare, Kyoto, Japan). During the measurement pauses, the volunteers were asked to rest, not to drink, not to visit the bathroom, and in particular not to practice any physical exertion, read, or undergo increased light exposure. Written informed consent was obtained from all patients, and the present study was approved by the ethical committee at the University of Basel, Switzerland, in accordance with the Declaration of
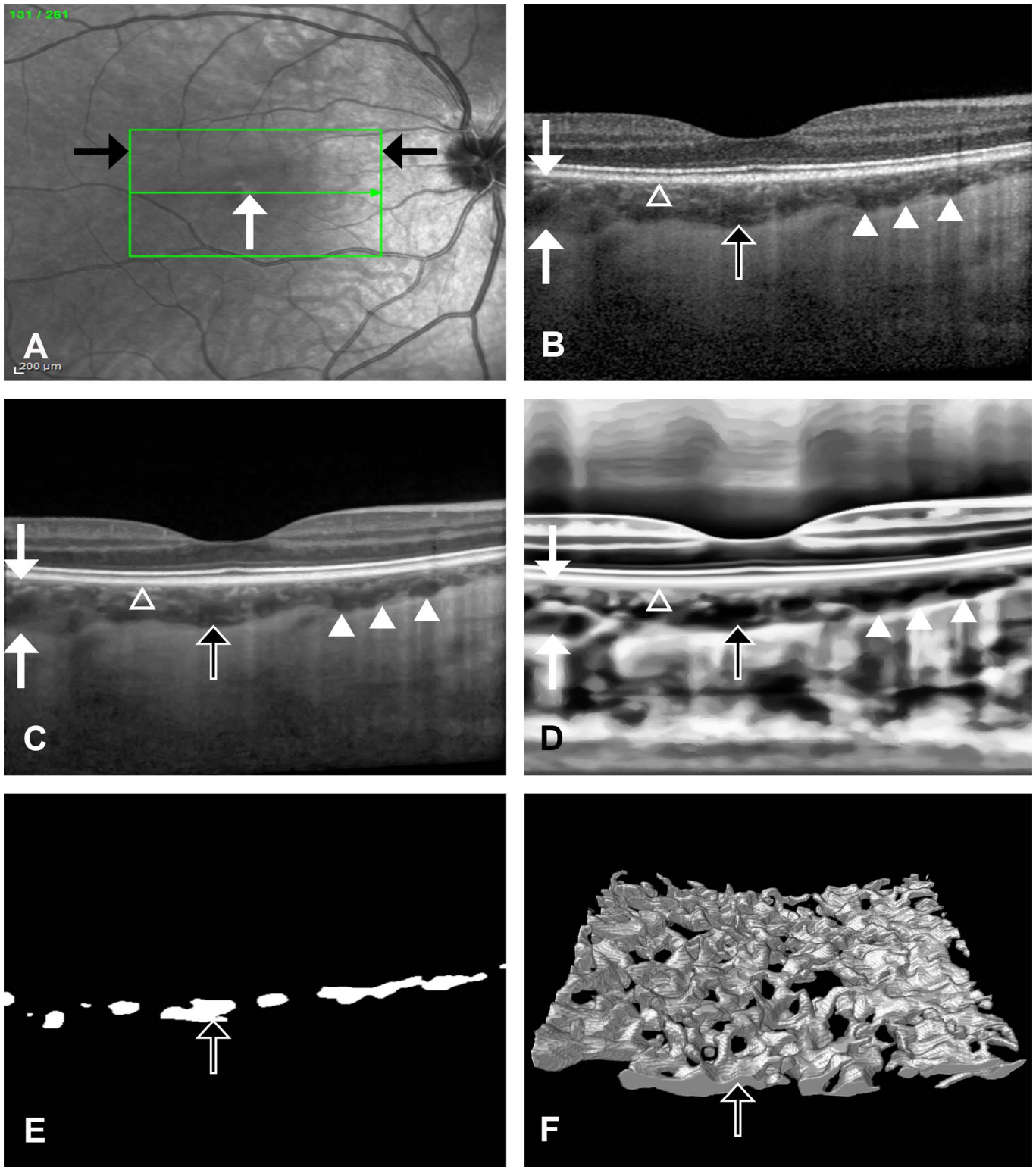
Figure 1. Illustration of speckle-noise freed choroidal angiography without the need for dye-injection in EDI-SDOCT with deep signal penetration into the choroid. (A) Scanning laser ophthalmoscopy (SLO) examination showing acquired retinal volume (*green box*, outlined with *black arrows*). The *white arrow* indicates the site of one single, cross-sectional EDI-OCT depicted in (B). Original EDI-OCT scan of the macula, centered on the foveola. The total choroid thickness is indicated with *two white arrows*. The choroid-sclera interface is

→

←
shown with *white triangles*. Choroidal vessels appear as hyporeflective, dark spaces (*black arrow*). Choroidal tissue is shown as hyperreflective (bright) rich branching bands (*white outlined triangle*). Note the granular aspect of this original EDI-OCT image caused by speckle-noise. (C) Same OCT scan as in (B) but speckle-noise freed. The choroidal compartments seem to be better outlined and enhanced. The central choroidal vessel look better demarcated (*black arrow*). The structure of the choroidal tissue is preserved (*white outlined triangle*) and the choroid-sclera interface (*white triangles*) seem easier to be detected. (D) Enhanced compartmentalization of the choroid into fluid filled spaces and tissue after image normalization, signal shadow removal, and overdriving histogram equalization based on the Contrast Limited Adaptive Histogram Equalization (CLAHE). (E) Vessel segmentation and extraction using threshold filtering in a single cross sectional OCT scan showing extracted choroidal vessels. (F) Three-dimensional model of the choroidal vessels constructed from collected single layer extractions (E).

Helsinki and in compliance with data protection regulations.

EDI-OCT Examination

A single experienced ophthalmologist imaged all choroidal volumes using a Heidelberg Spectralis (enhanced depth SDOCT, Spectralis HRA 2 Version 6.0.10.0; Heidelberg Engineering, Heidelberg, Germany). The scan pattern was raster lines $4.5 \times 3.0 \times 1.9$ mm, 261 B-Scans, distance between B-Scans of 12 µm with EDI-mode on. Imaging via OCT was averaged for 20 scans using the automatic averaging and tracking feature. The number of volume scans were ×6 for the right eye, ×1 for the left eye in each individual.

OCT Data Postprocessing and Speckle-Noise Removal

From the three-dimensional (3D) OCT data, the single B-scans were normalized using the shadow removal and contrast enhancement method,[30] and the aspect ratio was normalized. This resulted in OCT volumes with real-world aspect ratios in all three dimensions. The OCT data were freed from speckle noise with preservation of structural information.[31] To better separate hyperreflective from hyporeflective areas in the OCT volume, an overdriving histogram equalization based on the contrast limited adaptive histogram equalization method was used. Postprocessing was finished by two subsequent denoising runs.[32]

Compartmentalization of the Choroid (Vessel and Tissue Extraction)

For segmentation, only preprocessed OCT data were selected using an open source image-processing program (ImageJ; available in the public domain at http://imagej.nih.gov/ij/). An individual choroidal region of interest (ROI) reaching from the hyper-reflective band corresponding to the RPE to the outer surface of the choroid was defined in a first step.[33] This ROI was centered and applied to all consecutive individual OCT volumes and transferred manually to an approximately equal position of the fellow eye.

In the preprocessed volume, the hyporeflective choroidal vessels were segmented by threshold filtering in all volumes at a threshold level of 45. Analogously, choroidal tissue volume was obtained in the color-inverted OCT data.

Based on international OCT nomenclature, the hyporeflective choroidal formations (signal-poor areas) were considered as vascular choroidal spaces or fluid-filled spaces and analyzed (fluid inner space analysis [FISA]).[34] In contrast, the hyperreflective structures were defined as tissue and analyzed (tissue inner space analysis [TISA]). The postprocessing pipeline used in this study is shown in Figures 1A–F. Extraction of choroidal tissue and fluid-filled spaces of three different eyes are shown in Figure 2.

The metric volumes (mm^3) were converted from the extracted volumes of FISA and TISA in pixel space with respect to the real-world dimension and aspect ratio of the OCT C-scan.

Statistical Analysis

Short-Term Reproducibility

To define the reproducibility of our speckle noise-freed choroidal vessel extraction method, intraclass correlation (ICC) was chosen to define the intrasubject variability of six repeated measurements of the right eye within 1 hour. Data analysis included measurements of extracted FISA and TISA datasets of the right eye only. Intraclass correlation compares the intrasubject variability to the total variability. Usually, a coefficient over 0.8 is considered as a reliable result, thus reflecting a small subject variability in our case. Intraclass correlation was estimated with a 95% confidence interval (CI). Intraclass correlation data were calculated for lower and upper confidence limits (LCL, UCL), TISA, FISA, and a separate coefficient defined as total choroid ratio (TCR). Total choroid ratio is defined as the ratio from TISA data divided by the corresponding volume data of FISA. Therefore,
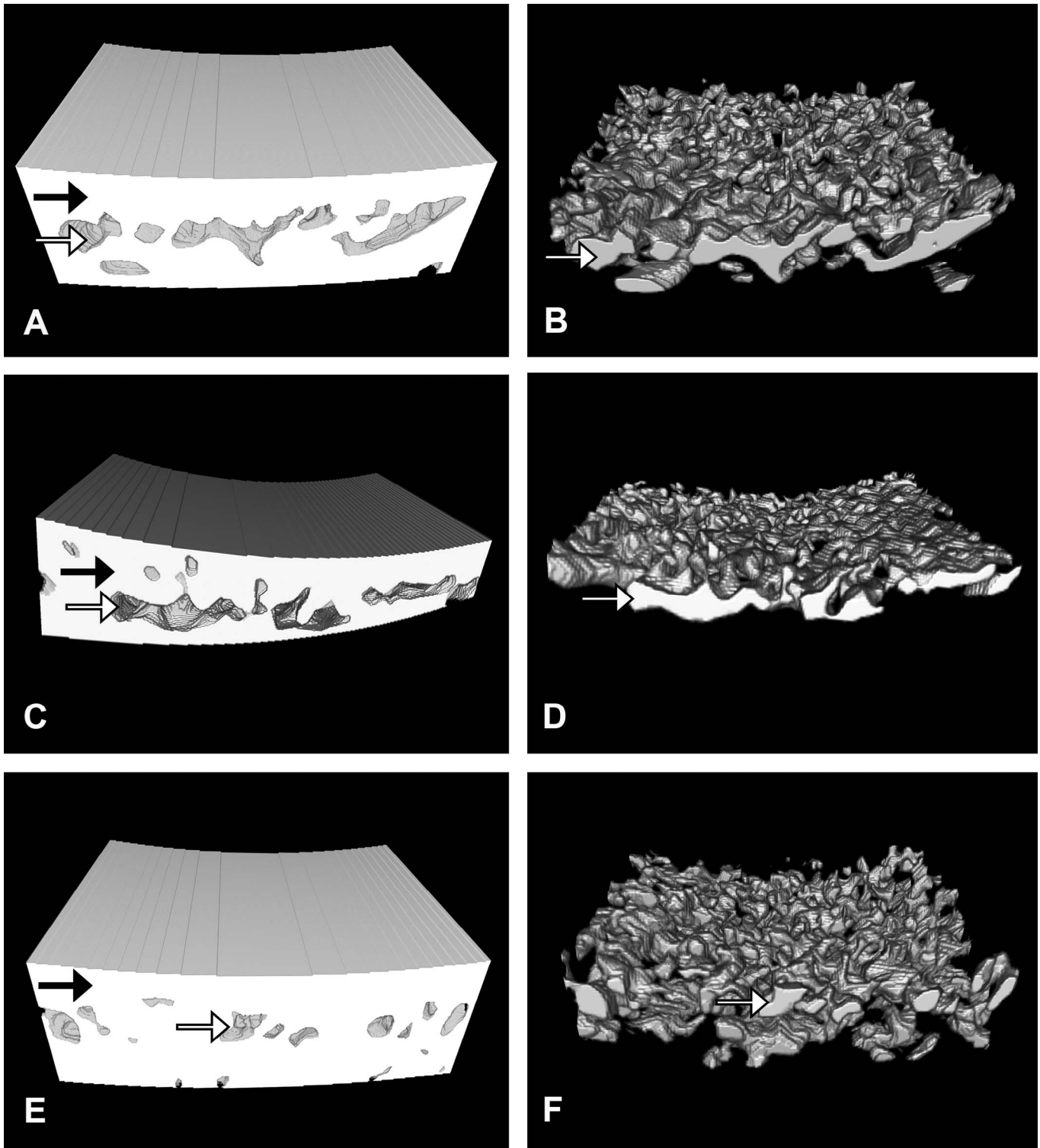
Figure 2. Illustration of the choroidal compartments of choroidal vessels ("fluid") and tissue provided by speckle-noise freed EDI-Spectral OCT of three different eyes. (A, C, E) Volume extractions of choroidal tissue shows the higher amount of tissue volume (*black arrows*) compared to vessel volume (*white arrows*). (B, D, F) Corresponding three-dimensional models of choroidal vessel extractions showing the large interindividual variation of biological tissue.

Table 1. Clinical Data in Study Subjects ($n = 13$) and Eyes ($n = 26$)

	Mean (SD)	Right Eye	Left Eye	P Overall	N
Age, y	22.0 (5.61)	22.0 (5.73)	22.0 (5.73)	1.000	26
BMI	20.8 (1.68)	20.8 (1.71)	20.8 (1.71)	1.000	26
RE, D	−0.41 (1.37)	−0.37 (1.34)	−0.46 (1.45)	0.862	26
AL	23.3 (0.76)	23.3 (0.76)	23.3 (0.79)	0.962	26
ACD	3.56 (0.20)	3.54 (0.21)	3.57 (0.20)	0.696	26
IOP	15.3 (2.13)	15.2 (2.08)	15.4 (2.26)	0.788	26
BP.sys	114 (9.64)				13
BP.dias	69.5 (6.58)				13
Pulse, min	68.1 (9.82)				13

RE, refractive error in Diopters; AL, axial length; ACD, anterior chamber depth; BP.sys, systolic blood pressure; BP.dia, diastolic blood pressure.

TCR describes a relation between choroidal tissue and vessels in the same measured choroidal volume. Data analysis was performed using Excel for Mac 2011 version 14.4.7, and R version 3.1.3.[35]

Descriptive Statistics

Descriptive statistics were performed by using all mean and standard deviations of TISA, FISA, and TCR.

Comparison Between Right and Left Eyes

Side comparison was performed using a linear mixed-effects model for mean TISA data, mean FISA data, and TCR results.

Body Mass Index (BMI)

The BMI represents a statistically developed measure based on data derived from height (h, cm) and weight (w, kg) and was calculated using the formula $BMI = x/(y \times y)$, where $x =$ bodyweight in kg and $y =$ height in m. In most cases, a BMI for adults between 18.5 to 24.9 is considered as a normal weight by the World Health Organization.[36]

Results

Macular OCT volume scans of 26 consecutive eyes (13 right, 13 left) from 13 healthy females were measured in this study. Measurement times were early morning (8–10 AM), approximately noon (10 AM to 2 PM), and late afternoon (2–5 PM) in five, four, and four participants, respectively. Mean patient age was 22 years (range, 19–22 years). Mean BMI was 20.8. Mean refractive error was −0.41 diopters, mean central axial length was 23.3 mm, mean anterior chamber depth was 3.56 mm, and mean IOP was 15.3

Table 2. Overview of All Measured Volumes and Total Choroid Ratios in All Subjects ($n = 13$)

	FISA OD	TISA OD	TCR OD	FISA OS	TISA OS	TCR OS
1	657,703,263.8	3,652,022,543	5.552690315	636,103,124.8	3,667,557,771	5.76566539
2	474,415,455.3	3,172,565,705	6.687315242	743,183,955.4	3,192,173,598	4.295267107
3	579,909,355.9	3,607,150,071	6.220196371	570,869,875.7	3,455,315,090	6.052719258
4	609,524,809.6	2,967,361,169	4.868318931	572,063,306	3,199,708,389	5.59327675
5	662,386,382.7	3,320,042,329	5.012244237	810,519,736.6	3,182,740,745	3.926789937
6	474,318,863.4	3,342,432,539	7.046805002	591,850,638.4	3,645,039,319	6.158714855
7	289,359,474.4	2,553,209,621	8.823660004	334,302,219.5	2,530,227,814	7.568683863
8	517,945,612.7	3,482,953,724	6.724554931	665,139,337.9	3,522,838,390	5.296391583
9	623,326,659.6	2,732,893,098	4.38436742	647,989,541.3	2,708,230,217	4.179435074
10	485,342,845.1	2,442,485,194	5.03249449	504,847,454.2	2,440,705,059	4.834539698
11	584,717,004	4,691,567,365	8.023654748	635,456,149.2	4,714,077,837	7.418415642
12	947,016,596.1	4,956,289,323	5.233582329	614,064,183.7	3,084,340,131	5.022830206
13	633,272,332.9	4,314,380,610	6.812836099	631,456,078.7	4,316,196,864	6.835308123

Units are for FISA and TISA μm^3.

Table 3. Analysis of All Mean and SDs of TISA, FISA, and TCR

	All $N = 90$	#1 $N = 13$	#2 $N = 13$	#3 $N = 13$	#4 $N = 13$
FISA mm^3	0.58 (0.14)	0.58 (0.15)	0.58 (0.16)	0.59 (0.15)	0.58 (0.14)
TISA mm^3	3.45 (0.72)	3.49 (0.79)	3.49 (0.77)	3.47 (0.77)	3.48 (0.78)
TCR	6.13 (1.34)	6.25 (1.36)	6.25 (1.40)	6.02 (1.13)	6.13 (1.16)

#1–7 = obtained OCT volumes (#1–6 repeated measurements of the right eye, #7 volumes of the left eye).

mm Hg. Mean systemic diastolic blood pressure was 69.5 mm Hg. Mean systolic blood pressure was 114 mm Hg, and mean pulse was 68.1 per minute. No significant differences between sides with respect to diopters, anterior chamber depth, IOP, or systemic blood pressure were found. The clinical data are summarized in Table 1.

Reproducibility FISA, TISA, TCR

In six repeated measurements of the right eye, FISA within 1 hour had an ICC of 95.15% (90.01–

Figure 3. Chart of measured choroidal vessel volumes of the right eye (A) and the left eye (B). FISA, *dark columns*; TISA, *bright columns*; TCR, calculated by dividing TISA by FISA. The differences in choroidal layers between subjects was caused mainly due to alterations in choroidal tissue.

98.24). The ICC of TISA was 99.75% (99.47–99.91), and the TCR had an ICC of 88.84% (78.28–95.82). The interindividual coefficient of variation (CV) was 22%.

Comparison of Left to Right Eyes

The FISA difference was 0.033 (95% CI −0.0018–0.0680, $P = 0.063$), TISA was −0.118 (CI −0.2373–0.0023, $P = 0.055$), TCR was −0.590 (CI −0.9047 to −0.2754, $P = 0.004$). The ICC for FISA and TISA showed a trend in the difference when comparing the left and right eyes, respectively. However, the TCR showed a significant difference between the eyes in the measured area ($P < 0.001$).

Descriptive Statistics

Mean overall FISA was 0.58 mm^3 (range, 0.25–0.98 mm^3, SD = 0.14); mean TISA was 3.45 mm^3 (range, 2.38–5.0 mm^3, SD .072); mean TCR was 6.13 (overall range, 3.93–10.2 mm^3, SD = 1.34). The volume data of TISA and FISA and the corresponding TCR ratio are shown in Table 2. Analysis of all mean and SDs of TISA, FISA, and TCR are summarized in Table 3. Figures 3 to 5 show results from the data analysis.

Discussion

A total of 26 healthy eyes from 13 healthy young females were enrolled for choroidal OCT analysis in this study. This resulted in 78 volumes of OCT data sets for the right eye and 13 volumes for the left eye, respectively. With respect to parameters, such as axial length of the eye, anterior chamber depth, IOP, or systemic blood pressure, no significant correlation to the choroidal data could be found in the ultra–short-term measurements performed.

In this study, we observed for the first time to our knowledge a very high reproducibility of speckle-noise freed spectral domain OCT choroidal angiography using a commercially available and widespread OCT
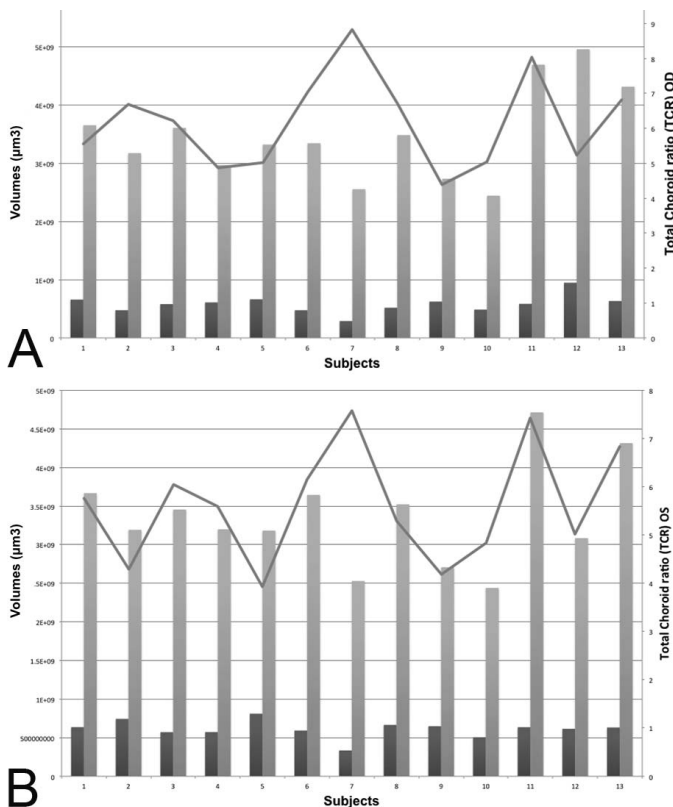
Table 3. Extended

	#5 N = 13	#6 N = 12	#7 N = 13	P Overall	N
FISA mm^3	0.58 (0.15)	0.54 (0.12)	0.61 (0.11)	0.939	90
TISA mm^3	3.47 (0.79)	3.37 (0.65)	3.36 (0.65)	0.998	90
TCR	6.20 (1.69)	6.45 (1.52)	5.61 (1.18)	0.825	90

system. Previous investigators have researched automated segmentation and analysis of choroidal thickness and volume. They reported an ICC of 0.98 by SSOCT and 0.73 to 0.97 by SDOCT.[37–39] The reproducibility was determined in other studies using SDOCT with an ICC of approximately 0.87 to 0.992 for retinal thickness measurements and macular ganglion cell analysis, respectively.[40,41] Compared to these studies, our results, obtained from speckle-noise freed EDI-OCT are in the superior range and seem to be highly reliable, repeatable, and reproducible. Our results are significant because we may add a novel algorithm to the already established image processing methods.

To our knowledge, this is the first study of a quantitative endoluminal assessment of choroidal vessels and their surrounding choroidal tissue, thus offering data and an illustration about the choroidal compartments of "fluid" and "tissue." We found an average ratio between choroidal tissue to vessels (TCR) of 6.13 with a large interindividual variation from 3.93 to 10.2. It was interesting to detect that the choroidal vessel volume did not show a pronounced interindividual difference, but the difference between subjects with regard to the choroidal layers was mainly caused by alterations in the amount of choroidal tissue.
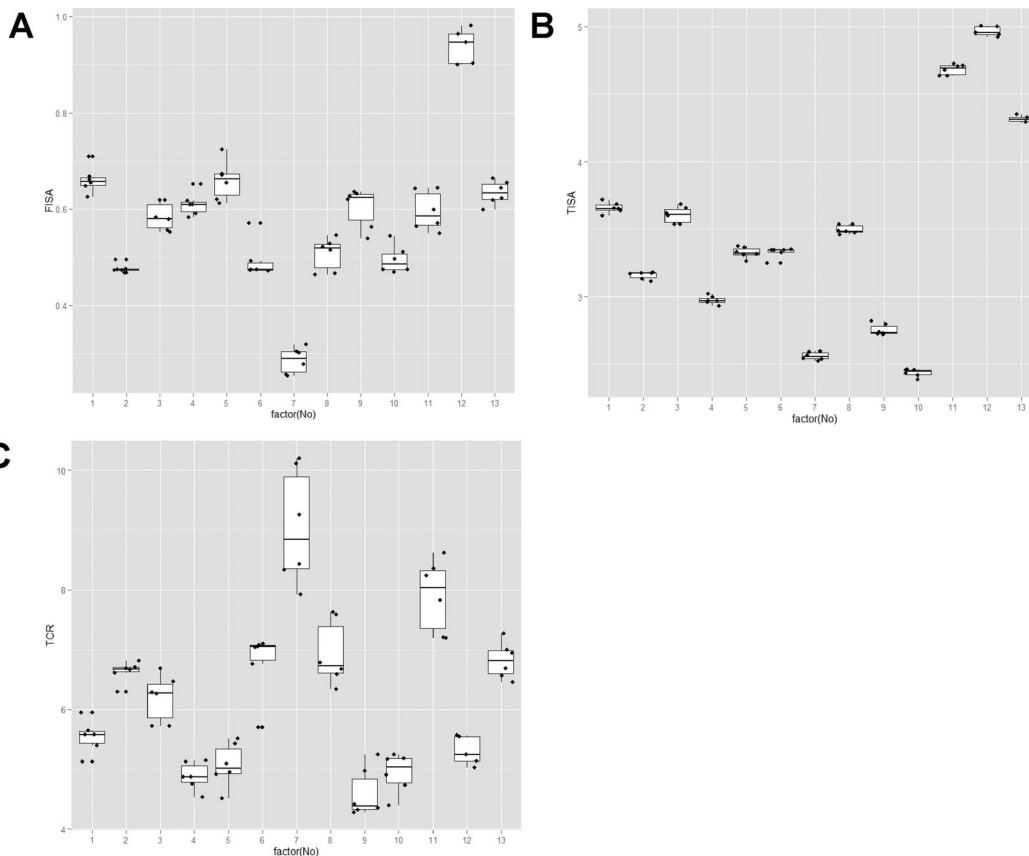
The comparison between sides showed significant

Figure 4. Box plot graphs of macular choroidal volumes measured as extracted volumes of FISA (A), TISA (B), and TCR by dividing TISA by FISA (C) in 13 healthy subjects. Data of TISA show minimal interindividual variation, compared to FISA and TCR.
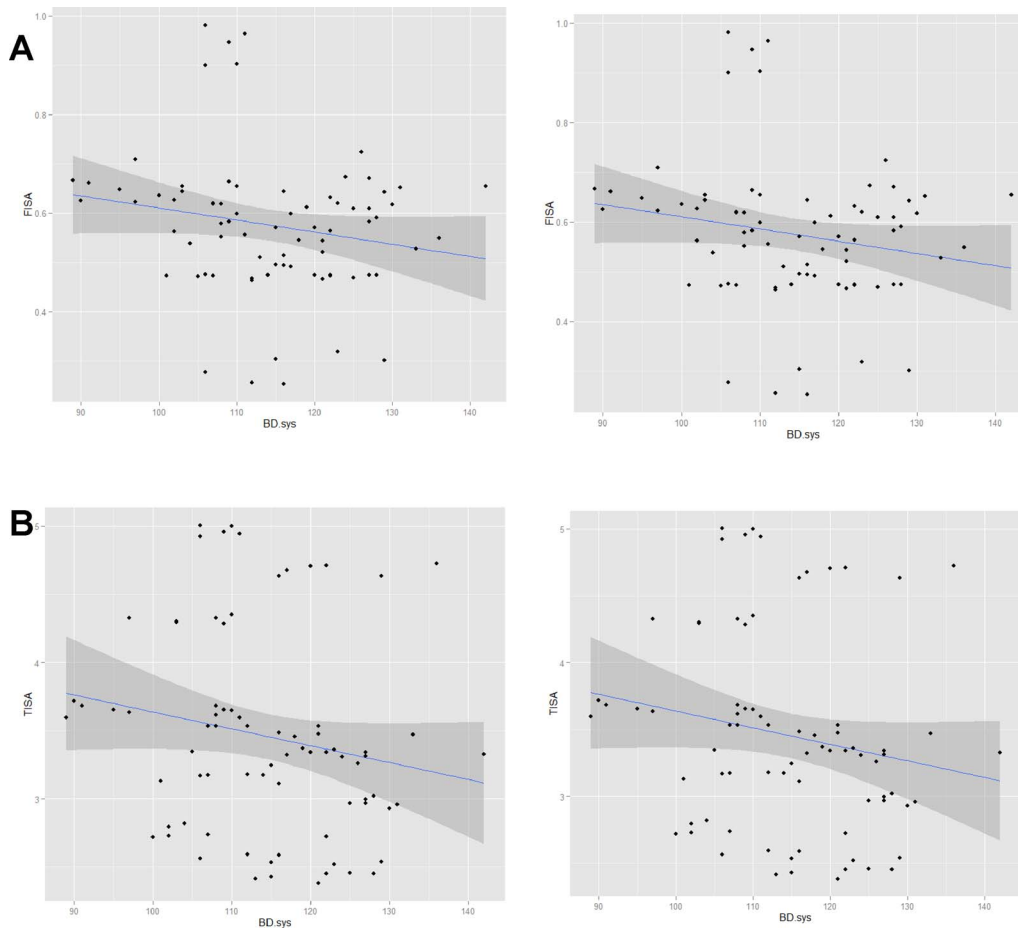
Figure 5. Scatter plot graph of overall FISA (A) and TISA data (B) against measured data of systolic and diastolic blood pressure. *Blue line* shows regression line. Apparently, no dependency in the repeated measurements within 1 hour between blood pressure and the acquired volumes can be detected.

differences in the measured ROI. This could be caused by real, existing, structural differences or more probably because of manual malpositioning of the ROI. Thus, it has to be emphasized that, concerning side differences, corresponding ROI have to be placed with caution in future studies.

There are several limitations to this study. One data set in one person had to be excluded for statistical analysis because the data acquisition exceeded the allowed measuring time and was terminated by the OCT system automatically; in that case the data could not be fully measured. All other 90 datasets were investigated. The image quality was enhanced by using the EDI mode and the averaging of 20 images; however, this resulted in a very long acquisition time using spectral-domain OCT, in some cases up to 3 minutes for a single, high quality retinal OCT volume. Yet, even with these very cooperative individuals, multiple breaks

had to be inserted to obtain the concentration upright and keep the cornea well moistened. Therefore, the mentioned OCT settings are only helpful in subjects with a very good central fixation and perfect cooperation. Another limitation was the relative small number of subjects and the restriction to include only young more-or-less emmetropic females. Future studies using a larger number of patients would help to clarify variations between sex, age, and different diseases. Still, our cohort is representative for a population of young healthy women.

The great opportunity and strength of the speckle-noise freed OCT method described was that it allowed to image and characterize not only choroidal vessels without the need for dye-injection but even choroidal tissue. This could be helpful in cases with pathologic tissue growth such as choroidal tumors or fluid accumulations. Since this is a postprocessing tool,

the technique may potentially be used on all 3D OCT data. The analysis of volume data would benefit from OCT data with a good resolution and with little motion artifacts. Theoretically, faster and better OCT systems also should improve the quality of OCT images and, thus, contribute to a better visualization of choroid in the future.

Since the technology generates three-dimensional signal vector paths for tracing the spatial OCT information, it is self-explanatory that the method can only be used on OCT volume data and not on isolated, two-dimensional B-scans. A major problem of the spectral OCT measurements was that sometimes very large differences occur in the illumination of the various B-scans within the same OCT volume. These differences had to be balanced automatically by the algorithm to continue image processing and may be a source of artifacts. To better outline choroidal spaces, the contrast of the image was increased, which in turn could lead to artifacts. Another limitation of speckle-noise freed imaging and vessel extraction is the current lack of a widely accepted level for an exact threshold filtering. A low threshold shows the core areas of the vessels quite accurately, but loses the lateral delimitation, so that the vessel volume is displayed as artificially small. On the other hand, a high level fills many vessels, but areas outside the actual vessel structure potentially are flooded as well and the real vessel volume could be overestimated. However, in this study the same postprocessing settings were used for all volumes, so that in subsequent new findings, the volumes could be adapted easily. Therefore, comparative studies are necessary to define a single threshold filtering level and to explore possible artifacts in detail. There is a discussion as to whether fully automated segmentation systems provide better results. We rather propose to use complementary systems where the physician is not confronted with a "self-running black box" but decides what is to be measured and the rest is performed by a computer. This complementary approach allows better control of processes and also should help to prevent errors in the evaluation of diseases.

In conclusion, we described a novel, very reproducible, speckle-noise freed OCT choroidal angiography and choroidal tissue characterization method in healthy young females. The results indicated that speckle-noise removal from OCT images may be used as an adjunctive illustrative imaging tool in the evaluation of choroidal and retinal pathologies and may provide additional 3D information about the choroid. We hope that our new approach will improve OCT image quality to favor diagnosis and monitoring and, thus, the prognosis of diseases.

Acknowledgments

References

1. Parver LM, Auker C, Carpenter DO. Choroidal blood flow as a heat dissipating mechanism in the macula. *Am J Ophthalmol*. 1980;89:641e6.
2. Alm A, Bill A. Ocular and optic nerve blood flow at normal and increased intraocular pressures in monkeys (*Macaca irus*): a study with radioactively labelled microspheres including flow determinations in brain and some other tissues. *Exp Eye Res*. 1973;15:15e29.
3. Spaide RF, Koizumi H, Pozzoni MC. Enhanced depth imaging spectral-domain optical coherencetomography. *Am J Ophthalmol*. 2008; 146:496–500.
4. Drexler W, Fujimoto JG. State-of-the-art retinal optical coherence tomography. *Prog Retina Eye Res*. 2008; 27:45–88.
5. Sander B, Larsen M, Thrane L, et al. Enhanced optical coherence tomography imaging by multiple scan averaging. *Br J Ophthalmol*. 2005; 89: 207–212.
6. Chhablani J, Barteselli G, Wang H, et al. Repeatability and reproducibility of manual choroidal volume measurements using enhanced depth imaging optical coherence tomography. *Invest Ophthalmol Vis Sci*. 2012 53:2274–2280.
7. Sanchez-Cano A, Orduna E, Segura F, et al. Choroidal thickness and volume in healthy young white adults and the relationships between them and axial length, ammetropy and sex. *Am J Ophthalmol*. 2014;158:574–583.

8. Fein JG, Branchini LA, Manjunath V, et al. Analysis of short-term change in subfoveal choroidal thickness in eyes with age-related macular degeneration using optical coherence tomography. *Ophthalmic Surg Lasers Imaging Retina*. 2014;45:32–37.

9. Imamura Y, Fujiwara T, Margolis R, et al. Enhanced depth imaging optical coherence tomography of the choroid in central serous chorioretinopathy. *Retina*. 2009;29:1469–1473.

10. Manabe S, Shiragami C, Hirooka K, et al. Change of regional choroid thickness after reduced-fluence photodynamic therapy for chronic central serous chorioretinopathy. *Am J Ophthalmol*. 2015;159:644–651.

11. Nagasawa T, Mitamura Y, Katome T, et al. Macular choroidal thickness and volume in healthy pediatric individuals measured by swept-source optical coherence tomography. *Invest Ophthalmol Vis Sci*. 2013;54:7068–7074.

12. Read SA, Collins MJ, Vincent SJ, Alonso-Caneiro D. Choroidal thickness in myopic and nonmyopic children assessed with enhanced depth imaging optical coherence tomography. *Invest Ophthalmol Vis Sci*. 2013;54:7578–7586.

13. Ikuno Y, Tano Y. Retinal and choroidal biometry in highly myopic eyes with spectral-domain optical coherence tomography. *Invest Ophthalmol Vis Sci*. 2009;50:3876–3880.

14. Troilo D, Nickla DL, Wildsoet CF. Choroidal thickness changes during altered eye growth and refractive state in a primate. *Invest Ophthalmol Vis Sci*. 2000;41:1249–1258.

15. Nickla DL, Wildsoet CF, Troilo D. Diurnal rhythms in intraocular pressure, axial length, and choroidal thickness in a primate model of eye growth, the common marmoset. *Invest Ophthalmol Vis Sci*. 2002;43:2519–2528.

16. Stone RA, Quinn GE, Francis EL, et al. Diurnal axial length fluctuations in human eyes. *Invest Ophthalmol Vis Sci*. 2004;45:63–70.

17. Loewen NA, Liu JH, Weinreb RN. Increased 24-hour variation of human intraocular pressure with short axial length. *Invest Ophthalmol Vis Sci*. 2010;51:933–937.

18. Chakraborty R, Read SA, Collins MJ. Diurnal variations in axial length, choroidal thickness, intraocular pressure, and ocular biometrics. *Invest Ophthalmol Vis Sci*. 2011;52:5121–5129.

19. Rahman W, Chen FK, Yeoh J, et al. Repeatability of manual subfoveal choroidal thickness measurements in healthy subjects using the technique of enhanced depth imaging optical coherence tomography. *Invest Ophthalmol Vis Sci*. 2011;52:2267–2271.

20. Tan CS, Ouyang Y, Ruiz H, Sadda SR. Diurnal variation of choroidal thickness in normal, healthy subjects measured by spectral domain optical coherence tomography. *Invest Ophthalmol Vis Sci*. 2012;53:261–266.

21. Mansouri K, Medeiros FA, Marchase N, et al. Assessment of choroidal thickness and volume during the water drinking test by swept-source optical coherence tomography. *Ophthalmology*. 2013;120:2508–2516.

22. Esmaeelpour M, Povazay B, Hermann B, et al. Mapping choroidal and retinal thickness variation in type 2 diabetes using three dimensional 1060-nm optical coherence tomography. *Invest Ophthalmol Vis Sci*. 2011;52:5311–5316.

23. Mansouri K, Medeiros FA, Tatham AJ, et al. Evaluation of retinal and choroidal thickness by swept-source optical coherence tomography: repeatability and assessment of artifacts. *Am J Ophthalmol*. 2014;157:1022–1032.

24. Adhi M, Ferrara D, Mullins RF, et al. Characterization of choroidal layers in normal aging eyes using enface swept-source optical coherence tomography. *PLoS One*. 2015;10:e0133080.

25. Hirata M, Tsujikawa A, Matsumoto A, et al. Macular choroidal thickness and volume in normal subjects measured by swept source optical coherence tomography. *Invest Ophthalmol Vis Sci*. 2011;52:4971–4978.

26. Považay B, Bizheva K, Hermann B, et al. Enhanced visualization of choroidal vessels using ultrahigh resolution ophthalmic OCT at 1050 nm. *Opt Exp*. 2003;11:1980–1986.

27. Esmaeelpour M, Ansari-Shahrezaei S, Glittenberg C, et al. Choroid, Haller's, and Sattler's layer thickness in intermediate age-related macular degeneration with and without fellow neovascular eyes. *Invest Ophthalmol Vis Sci*. 2014;22;55(8):5074–5080.

28. Haas P, Esmaeelpour M, Ansari-Shahrezaei S, et al. Choroidal thickness in patients with reticular pseudodrusen using 3D 1060-nm OCT maps. *Invest Ophthalmol Vis Sci*. 2014;55:2674–2681.

29. Esmaeelpour M, Ansari-Shahrezaei S, Glittenberg C, et al. Choroid, Haller's, and Sattler's layer thickness in intermediate age-related macular degeneration with and without fellow neovascular eyes. *Invest Ophthalmol Vis Sci*. 2014;55:5074–5080.

30. Girard MJ, Strouthidis NG, Ethier CR, Mari JM. Shadow removal and contrast enhancement in optical coherence tomography images of the

human optic nerve head. *Invest Ophthalmol Vis Sci*. 2011;52:7738–7748.

31. Gyger C, Hasler P, Cattin R, Maloca P. Three-dimensional speckle reduction in optical coherence tomography through structural guided filtering. *Opt Eng*. 2014;53:073105.

32. Pizer SM, Amburn EP, Austin JD, et al. Adaptive histogram equalization and its variations. *Comput Vision Graph*. 1987;39:355–368.

33. ImageJ, version 1.48b, Java 1.6.0_24 (64bit). Available at: http://imagej.nih.gov/ij/. Last download December 9, 2013.

34. Staurenghi G, Sadda S, Chakravarthy U, Spaide RF. International nomenclature for optical coherence Tomography. *Ophthalmology*. 2014;121:1572–1578.

35. R Core Team. *R: A Language and Environment for Statistical Computing*. Vienna, Austria: R Foundation for Statistical Computing; 2015. Available at: http://www.R-project.org/. Last accessed July 17, 2015.

36. WHO Body Mass Index. Available at: http://www.euro.who.int/en/health-topics/disease-prevention/nutrition/a-healthy-lifestyle/body-mass-index-bmi. Last accessed July 20, 2015.

37. Sim DA, Keane PA, Mehta H, et al. Repeatability and reproducibility of choroidal vessel layer measurements in diabetic retinopathy using enhanced depth optical coherence tomography. *Invest Ophthalmol Vis Sci*. 2013;54:2893–2901.

38. Zhang L, Buitendijk GH, Lee K, et al. Validity of automated choroidal segmentation in SS-OCT and SD-OCT. *Invest Ophthalmol Vis Sci*. 2015;56:3202–3211.

39. Gupta P, Sidhartha E, Girard MJ, et al. A simplified method to measure choroidal thickness using adaptive compensation in enhanced depth imaging optical coherence tomography. *PLoS One*. 2014;9:e96661.

40. Kim KE, Yoo BW, Jeoung JW, et al. Long-Term reproducibility of macular ganglion cell analysis in clinically stable glaucoma patients. *Invest Ophthalmol Vis Sci*. 2015;56:4857–4864.

41. Vazirani J, Kaushik S, Pandav SS, et al. Reproducibility of retinal nerve fiber layer measurements across the glaucoma spectrum using optical coherence tomography. *Indian J Ophthalmol*. 2015;63:300–305.

translational vision science & technology